Monitoring the behaviour of polymer fibres under axial compression

C. Vlattas and C. Galiotis†

Department of Materials, Queen Mary and Westfield College, Mile End Road, London E1 4NS, UK

(Received 20 August 1990; revised 13 November 1990; accepted 14 November 1990)

A modified version of the bending-beam technique was used to apply small and defined axial compressive loads to single polymer fibres spun from liquid-crystalline solutions. By monitoring the Raman frequencies along the fibre with a laser Raman microprobe, the critical compressive strain required for first fibre failure, as well as the molecular deformation in the post-failure region, could be assessed. In addition, estimates of the compression modulus and the critical compressive stress to failure were derived by determining the strain dependence of Raman frequencies of individual fibres in both tension and compression. The results showed that the compression modulus was generally lower than the tensile modulus, whereas the critical compressive stress to failure fluctuated between 290 MPa to 420 MPa over a wide range of moduli.

(Keywords: aramid fibres; Kevlar fibres; PBZT fibres; laser Raman spectroscopy; cantilever beam; compression modulus; tensile modulus; critical compressive strain; critical compressive stress; fibre microbuckling)

INTRODUCTION

It is now well established that polymer fibres and in particular polymer fibres spun from liquid crystalline solutions are relatively weak in compression[1]. A theoretical compressive strength equal to the longitudinal shear modulus of the fibre has been calculated using an elastic buckling analysis[2]. In practice however, the compressive strength appears to be lower than the shear modulus by a factor of about 3 (ref. 3) and no satisfactory explanation for this discrepancy has been proposed. Furthermore, there is a strong indication from values derived from testing of full composites that the compression modulus of a whole range of liquid crystalline polymer (LCP) fibres is significantly lower than the corresponding tensile modulus[1]. The situation is further complicated by the lack of a test method that can unambiguously assess the overall intrinsic properties of single filaments under axial compression. Indeed, none of the available tests measure the compressive strength directly, but they infer the critical compressive stress or strain to failure using assumptions about the loading condition and deformation process. These tests include the elastica loop test[4–6], the embedded fibre method[7], the recoil test[8] and the bending beam method[9].

In the elastica loop test[4–6] a loop is induced in a fibre which is trapped in an oil immersion between two microscope slides and, then, by pulling the two ends of the fibre, the loop is reduced gradually in size. In theory, the ratio of major to minor axis should stay constant ($=1.34$) as long as the fibre behaves elastically[2]. Any deviation would indicate that some form of non-Hookean behaviour takes place and, hence, the strain required for plastic deformation can be determined. Some of the problems related to this test are:

1. the difficulty in pulling such thin fibres;
2. the introduction of bending curvatures due to mishandling;
3. the difficulty in assessing the mode of failure;
4. the fact that only values of strain to failure can be derived.

The embedded fibre method is normally performed by incorporating single fibres in a polymer matrix and subsequently compressing the specimens parallel to the fibre axis, till fibre failure is detected by means of optical microscopy[7] or, more recently, laser Raman spectroscopy (LRS)[10]. Improvements to this method with reference to the measurements of the applied compressive strain in the vicinity of the fibre have been proposed by Van der Zwaag and Kampschoer[11]. Nevertheless, this method is extremely sensitive to fibre alignment and interfacial adhesion and can only provide estimates of compressive strain to failure.

In the recoil test a uniaxial compressive stress is assumed to be imparted to a filament by imposing 'snap-back' forces after controlled tensile failure[8]. Although this is a relatively new test and only preliminary data have been published[8,12], evidence has recently been provided[12] that the moving stress trajectory may not be uniaxial and, hence, affecting the mode of compressive failure. In addition, the determination of failure stress is not always straightforward and involves a long process of specimen inspection after failure[12].

The bending beam method was developed by DeTeresa *et al.*[9] and involves the application of well defined and uniform compressive strains to single filaments by bonding them to the compressive side of an elastic rectangular transparent polymer beam which is normally loaded in a cantilever configuration[9]. The fibres are glued onto the bars by means of a thin acrylic film which, in turn, transmits the load to the fibres and supports them against global (Euler) instabilities. Provided there is no slippage between the fibre and the bar, the maximum strain, $\varepsilon_{(x)}^{max}$, in the beam surface varies linearly along the length of the beam and is only a function of the position

Paper presented at Speciality Polymers '90, 8–10 August 1990, The Johns Hopkins University, Baltimore, MD, USA

† To whom correspondence should be addressed

0032-3861/91/101788-06

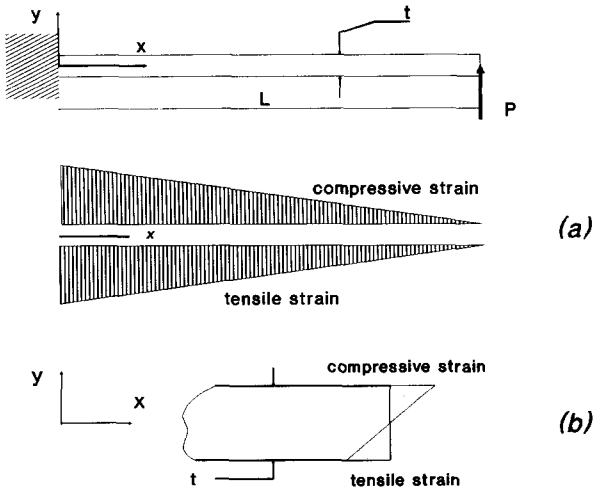

Figure 1 Distribution of (a) moment along the length, x, of the beam and (b) axial compressive and tensile strains across the thickness, y, of the beam

on the bar, x, as determined by the elastic beam theory[13]:

$$\varepsilon_{(x)}^{max} = \frac{3t\delta_{max}}{2L^2}\left(1 - \frac{x}{L}\right) \quad (1)$$

where L is the free length of the beam, t is the beam thickness and δ_{max} is the maximum deflection of the neutral axis of the beam at the point of application of load.

The loading geometry is shown in *Figure 1*. The fibres are examined in the compressed state by flexing the beam while making observations with an optical microscope. The critical compressive strain for first compressive failure, indicated by fibre kinking or microbuckling, is determined by simply measuring the distance from the clamped end to the point where the last kink band is seen[9]. As a result, the following drawbacks have been noted[9,14]: compressive failure could be detected only if a kink boundary is optically observed; the amount of film shrinkage and/or pre-stressed load on the fibre cannot be quantified; and only values of critical compressive strain to failure can be derived.

In this study, a modified version of the cantilever beam technique is employed to compress the fibres axially, while the molecular deformation of the embedded fibres under axial compression is monitored by scanning along the length of individual filaments with a laser Raman microprobe (*Figure 2*)[14]. Past work has shown that LRS can be used to measure the response of polydiacetylene[15,16], Kevlar[10,17], carbon[18] or poly(*p*-phenylene benzobisthiazole) (PBZT)[19] fibres to applied tensile load at the molecular level. In general, the Raman vibrational frequencies shift to lower values under tension[15–19] and to higher values under compression[10,14], and well defined relationships between Raman frequencies (molecular strain) and applied (macroscopic) strain can be obtained from a whole range of polymeric or polymer-derived fibres.

EXPERIMENTAL

Materials

Three different grades of commercial poly(*p*-phenylene terephthalamide) (Kevlar) fibres and a heat-treated PBZT fibre were tested in this study. The chemical formulae of the two types of fibres are illustrated in *Figure 3*. The tensile mechanical properties of all fibres are listed in *Table 1*.

Specimen preparation

The test specimens were prepared by aligning the single polymer filaments parallel to the length of poly(methyl methacrylate) (PMMA) bars and approximately at the centre of their width (*Figure 1*). The thickness and the

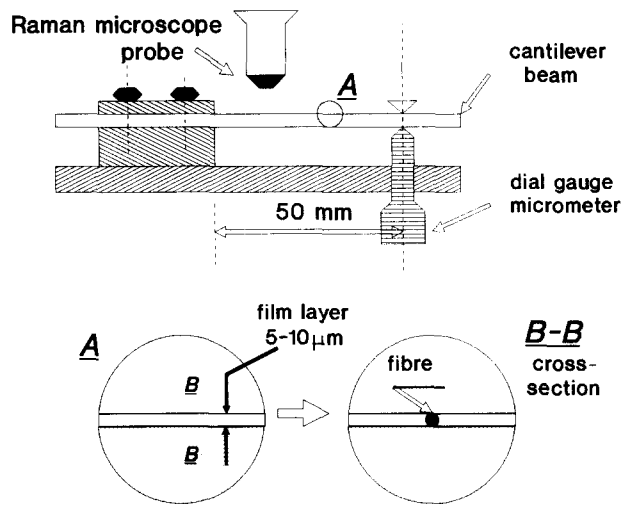

Figure 2 Schematic illustration of the cantilever rig assembly

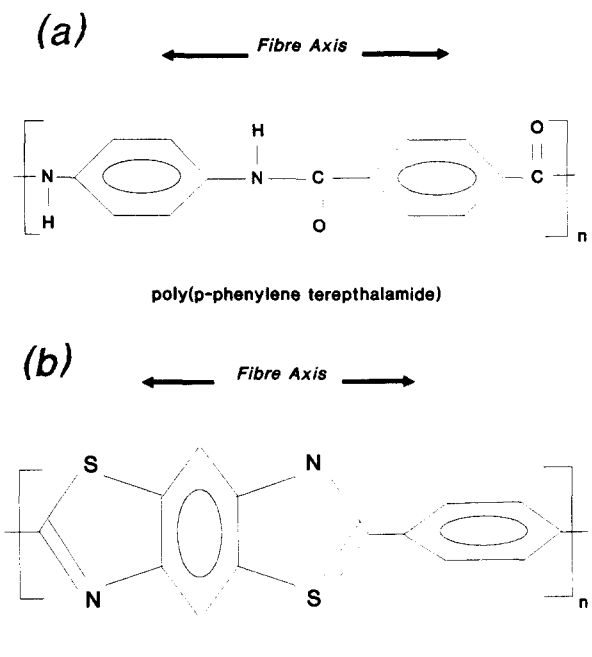

Figure 3 Chemical structures for (a) aramid and (b) PBZT fibres

Table 1 Tensile properties of Kevlar and PBZT fibres

Fibre	Tensile tangent modulus at 1%, E_t (GPa)	Fracture strain, ε_f (%)
Kevlar 29	80	3.0
Kevlar 49	130	2.5
Kevlar 149	160	1.2
PBZT	280	1.0

width of the beams were kept fixed at (5.5 ± 0.1) mm and (10.0 ± 0.1) mm, respectively. The free length of the beams was kept normally fixed at 50 mm. The fibres were bonded to the bars by spraying them with a thin clear acrylic (Krylon) adhesive. Care was taken to keep the thickness of the adhesive down to 10 μm so its effect on the elastic beam calculations was insignificant. The film was dried for several hours in a vacuum oven at room temperature.

Cantilever rig

The design of the cantilever rig is shown in *Figure 1*. The beam can be flexed up or down by means of a specially designed flat screw, subjecting the fibre to compression or tension, respectively. The fibres under load were examined with a laser Raman microscope which was located above the flexed beam, as shown in *Figure 2*.

Prior to cantilever compression testing, the Raman frequencies of all the embedded polymer fibres were recorded. All fibre specimens found to exhibit Raman frequency values different from the values of the stress-free fibre in air were discarded. Furthermore, any fibres that contained residual stresses due to either film shrinkage and/or mishandling were not included in the measurements.

Raman spectroscopy

Raman spectra were taken with the 514.5 nm line of an argon ion laser. A modified Nikon microscope was used to focus the incident laser beam to a 2 μm spot on the fibre. Care was taken not to exceed a maximum laser power of 1–2 mW on the sample to avoid local overheating of the fibre/acrylic film system. The 180° backscattered light was collected by the microscope objective and focused on the entrance slit of a SPEX 1877 triple monochromator. A Wright Instruments charge coupled device (CCD), cooled by liquid nitrogen, was employed as a photon counting system for recording the Raman spectra. All the Raman frequency values were derived by fitting Lorentzian routines to the CCD raw data.

RESULTS AND DISCUSSION

Raman spectra

The Raman spectrum of the Kevlar 49 fibre in the frequency region 1470–1690 cm^{-1} is given in *Figure 4*.

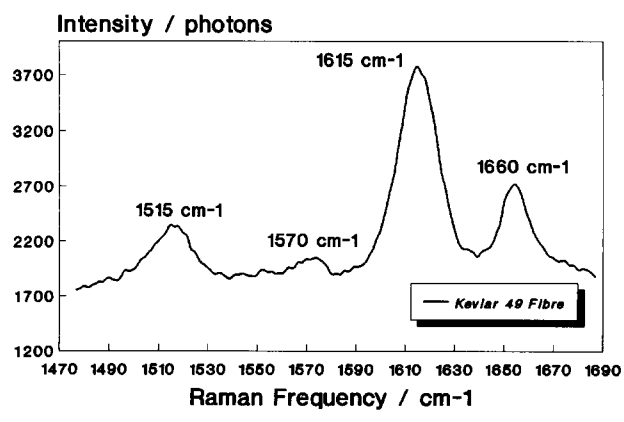

Figure 4 Raman spectra for a Kevlar 49 fibre in the 1470–1690 cm^{-1} frequency region

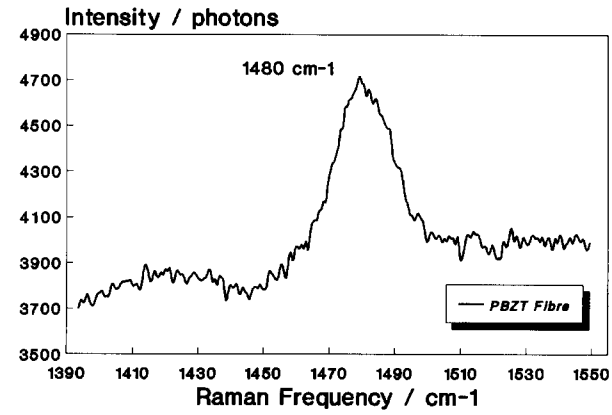

Figure 5 Raman spectra for a PBZT fibre in the 1390–1550 cm^{-1} frequency region

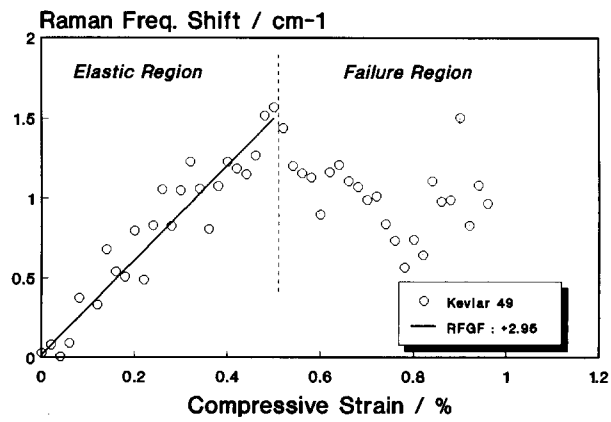

Figure 6 Raman frequency shift as a function of compressive strain for a Kevlar 49 fibre. ---, Onset of visible kink band formation

The intense band at 1615 cm^{-1} corresponds primarily to an in-plane benzene ring stretching vibration[20] (*Figure 3a*) and therefore is ideal for monitoring deformation effects in the polymer backbone. The Raman spectra for Kevlar 29 and 149 fibres are very similar as regards to the appearance of this band at approximately 1615 cm^{-1}. The Raman spectrum of the PBZT fibres, within the frequency region 1390–1550 cm^{-1}, is shown in *Figure 5* and is dominated by the band at 1480 cm^{-1} corresponding to an in-plane heterocyclic ring stretching vibration[21] (*Figure 3b*).

Compression tests

Typical cantilever compression plots are produced with the y-axis coordinate representing the Raman frequency difference or shift between the values obtained from the embedded part of the fibre and the values of the corresponding stress-free fibre in air, and with the x-axis coordinate representing the compressive strain calculated point-by-point along the fibre length (equation (1)). One such graph for a Kevlar 49 fibre is shown in *Figure 6*. As can be seen, up to 0.5% of applied compressive strain, the Raman frequency increases (to first approximation) linearly with compressive strain and then drops dramatically to much lower values. The initial linear increase of Raman frequency indicates that at least up to 0.5% of applied compressive strain, the intermolecular bonds are contracted by an amount which is approximately proportional to the macroscopic strain field. At about 0.55% of applied compressive strain the

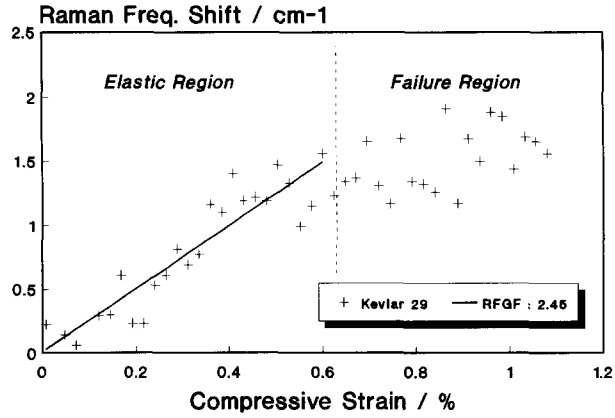

Figure 7 Raman frequency shift as a function of compressive strain for a Kevlar 29 fibre. ---, Onset of visible kink band formation

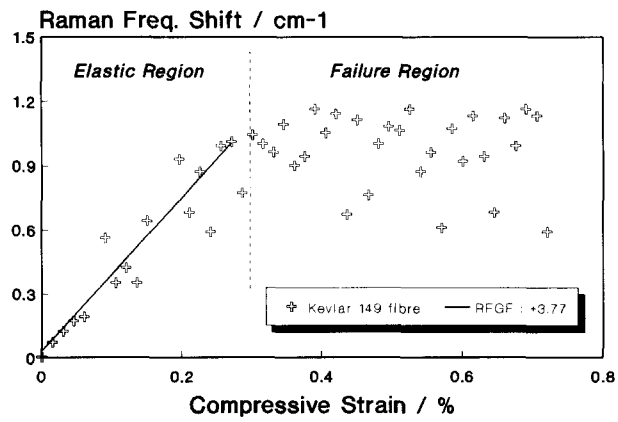

Figure 8 Raman frequency shift as a function of compressive strain for a Kevlar 149 fibre. ---, Onset of visible kink band formation

first kink band is formed as confirmed by microscopic observation. This causes a certain amount of intermolecular bond relaxation which, in turn, brings about the sudden drop of the corresponding Raman frequencies. This process is repeated at higher levels of applied strain as the fibre recovers some of the compressive strain between kink bands and relaxes again at subsequent failures.

The behaviour of the Kevlar 29 fibre shown in *Figure 7* is somewhat different. There is no sudden Raman frequency drop relating to fibre kinking which occurs just after 0.6% of applied compressive strain, instead the curve becomes increasingly non-linear exhibiting a considerable data scatter. This indicates that the molecules are still experiencing a significant amount of input compressive strain even within the kink-band zone.

In the case of Kevlar 149 fibre (*Figure 8*), a dramatic deviation from linearity is observed at an applied strain of approximately 0.3%, associated with the onset of fibre failure by kinking. Furthermore, the Raman frequencies at high applied compressive strains fluctuate widely around a plateau value. This indicates that the kink-band zone is smaller than in the case of Kevlar 49, and that the molecules adjacent to a kink band recover sharply to the value of compressive strain prior to failure. These observations have also been confirmed by complementary optical and electron microscopy studies[22].

Finally, the Raman frequency *versus* applied compressive strain for the PBZT fibre is shown in *Figure 9*. Again, the Raman frequency increases linearly up to the onset of first fibre failure which occurs by a bulging mechanism[22] at about 0.2% of compressive strain and then follows a regular pattern of peaks and troughs corresponding to recovery and failure regions, respectively. It is interesting to note that, like Kevlar 29 (*Figure 7*), the fluctuation of Raman frequency between successive recovery and failure regions is of relatively small magnitude indicating that the molecules within the bulging zone are still under a considerable amount of compressive strain.

Molecular deformation in both tension and compression

As mentioned earlier, the cantilever beam can also be flexed in the opposite direction subjecting the embedded fibre in a gradient of tensile load. By scanning along the fibre with the laser Raman probe, universal curves of Raman frequency *versus* applied strain can be produced in both tension and compression. Such curves are plotted in *Figures 10–13* for Kevlar 49, 29, 149 and PBZT fibres, respectively, and represent the molecular response of LCP fibres to an applied macroscopic strain. It can be clearly seen that almost all the fibres appear to be quite brittle in tension; the molecular deformation relates linearly to applied tensile strain all the way up to fracture. On the contrary the behaviour in compression is quite distinct, with all the fibres appearing to be 'yielding' at relatively low levels of applied compressive strain. It is interesting to note that in the case of Kevlar 49 (*Figure 10*), Kevlar 149 (*Figure 12*) and PBZT (*Figure 13*) fibres

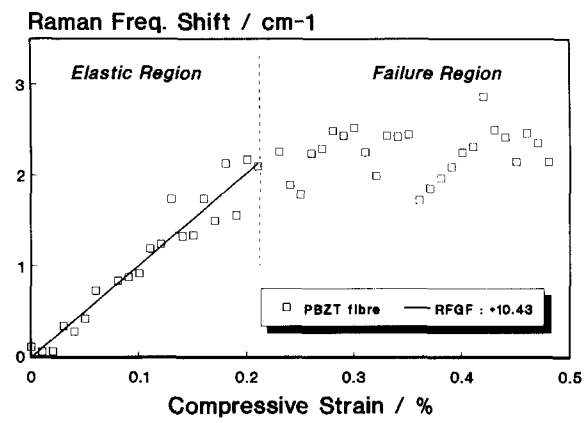

Figure 9 Raman frequency shift as a function of compressive strain for a PBZT fibre. ---, Onset of visible compression failure

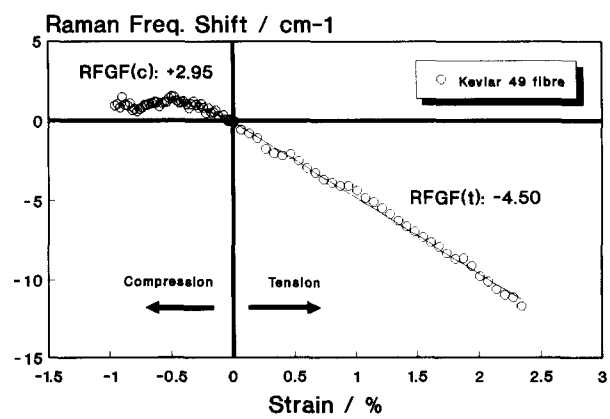

Figure 10 Raman frequency shift as a function of strain for a Kevlar 49 fibre under tension and compression cantilever beam loading

Table 2 Values of RFGF in tension and compression, estimated degree of modulus softening in compression, estimated modulus in compression, experimentally measured critical strain to failure and estimated critical compressive stress to failure

Fibre type	$RFGF_t$ ($cm^{-1}/\%$)	$RFGF_c$ ($cm^{-1}/\%$)	E_c/E_t	E_c^{est} (GPa)	ε_c (%)	σ_c^{est} (MPa)
Kevlar 49	−4.50	+2.95	0.55	85	0.45	382
	(±0.08)	(±0.19)			(±0.05)	
Kevlar 29 ($M_w = 1500$)	−2.67	+2.55	0.95	76	0.55	418
	(±0.05)	(±0.16)			(±0.05)	
Kevlar 149	−5.22	+3.78	0.72	115	0.25	287
	(±0.20)	(±0.41)			(±0.05)	
PBZT	−13.13	+10.43	0.79	222	0.15	333
	(±0.22)	(±0.61)			(±0.05)	

The experimental values represent averages from at least three fibres

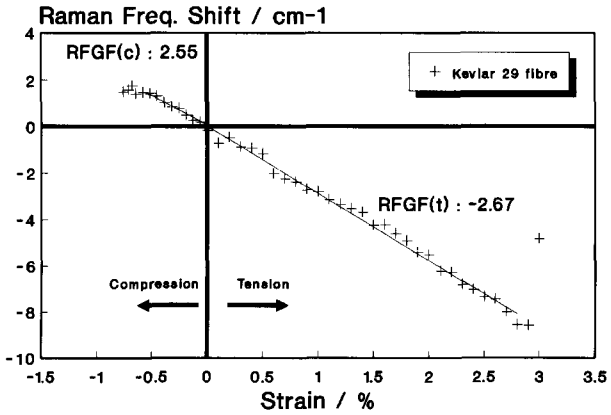

Figure 11 Raman frequency shift as a function of strain for a Kevlar 29 fibre under tension and compression cantilever beam loading

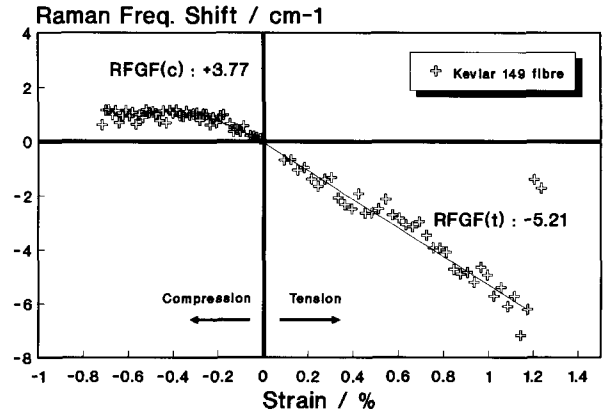

Figure 12 Raman frequency shift as a function of strain for a Kevlar 149 fibre under tension and compression cantilever beam loading

the overall tension–compression behaviour can be expressed by a single curve[22]. However, bearing in mind the resolution of these experiments and the considerable experimental scatter, the data in the tension and compression elastic regions of the graph are to first approximation least-squares-fitted here with straight lines. The slopes of these straight lines represent the Raman frequency gauge factors (RFGF) so-called as they describe the sensitivity of molecular deformation (bond extension or contraction) upon a given value of applied strain.

The RFGF values in both tension and compression for all the fibres tested are listed in *Table 2*. The values in compression are consistently lower than the values in tension. Indeed, as it has been argued elsewhere[14], in partially crystalline fibres, such as aramid or carbon, the macroscopic strain applied to a fibre is only partially effective in changing the interatomic separations, as part of the overall applied strain is consumed for crystallite rotation, shear, etc. Thus, the RFGF values measured for aramid[17] or carbon[18] fibres depend upon the degree of crystallinity, much in the same way as the modulus, and express the effectiveness of the applied load in extending or contracting the atomic bonds. For example, in the case of aramid fibres of different moduli, it has already been demonstrated[23] that the RFGF values in tension are directly proportional to the tensile modulus. Therefore, the reduction in the values of the RFGF in compression as compared to the values in tension, indicates that the compression modulus decreases with respect to the tensile modulus by an amount equal to the ratio of the RFGF values in compression and tension,

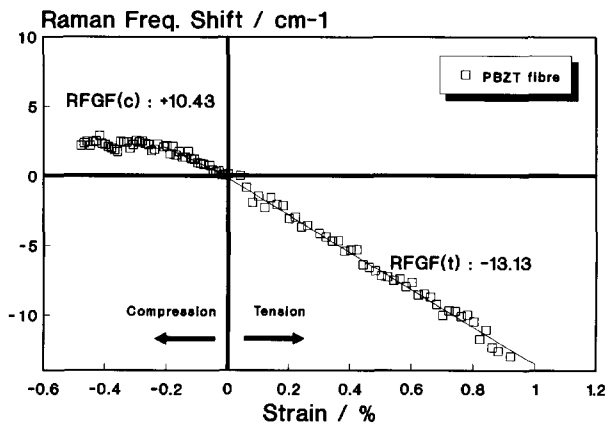

Figure 13 Raman frequency shift as a function of strain for a PBZT fibre under tension and compression cantilever beam loading

respectively. Indeed, if the fibre is regarded as a chain of crystallites, each having a slight misorientation with respect to the fibre axis, then the application of a tensile load will tend to align the crystallites to the loading direction. However, the application of compressive load will tend to align the crystallites normal to the loading direction. Furthermore, LCP fibres exhibit a microfibrillar structure, high degree of anisotropy and are extremely weak in the transverse direction. Therefore, when tested in compression, a greater portion of the applied compressive strain is expected to contribute towards shearing motions between crystallites rather than towards contracting individual bonds.

The estimated degree of modulus softening is shown in *Table 2*, as a ratio of compression to tension modulus (E_c/E_t). Hence, the estimated compression modulus E_c^{est} can be calculated from the formula

$$E_c^{est} = E_t \frac{(RFGF)_c}{(RFGF)_t} \quad (2)$$

where E_t is the tension modulus (*Table 1*) and $(RFGF)_c$ and $(RFGF)_t$ are the values of the least-squares-fitted slopes for the data of *Figures 10–13*, for compression and tension loading, respectively. The estimated compression modulus for a Kevlar 49 fibre is approximately 55% of its tensile modulus (*Table 1*), whereas the effect for the Kevlar 29 is less pronounced. Significant amounts of modulus softening are also estimated in the case of the higher modulus fibres such as Kevlar 149 and PBZT. These values of modulus softening for most of the fibres tested here agree well with values derived from testing of full composites[1].

By assuming a linear relationship between stress and strain at least up to the first compression failure estimates of the critical compressive stress σ_c^{est} can be produced from the formula:

$$\sigma_c^{est} = E_c^{est}\varepsilon_c \quad (3)$$

where E_c^{est} is the estimated compression modulus (equation (2)) and ε_c is the experimentally derived critical strain to compression failure. The values of σ_c^{est} are listed in *Table 2*, and in *Figure 14* the critical compressive stress to failure is plotted as a function of the estimated compression modulus. For the aramid fibres the values of critical compressive stress to failure appear to decrease by about 130 MPa as the modulus increases from 76 to 115 GPa. It is interesting to note that the corresponding critical compressive stress for the PBZT fibre with a compression modulus of about 220 GPa is approximately eight times lower than its corresponding tensile fracture strength. The values of compressive strength derived using this methodology, compare extremely well with the values obtained from composite testing and other methods[1]. This is remarkable bearing in mind the assumptions employed in this analysis. Although the tensile and compression moduli of the newly produced LCP fibres can now match the values obtained from carbon fibres[14], their compressive strength needs further improvement if these fibres are to compete successfully as reinforcements for composites in structural applications.

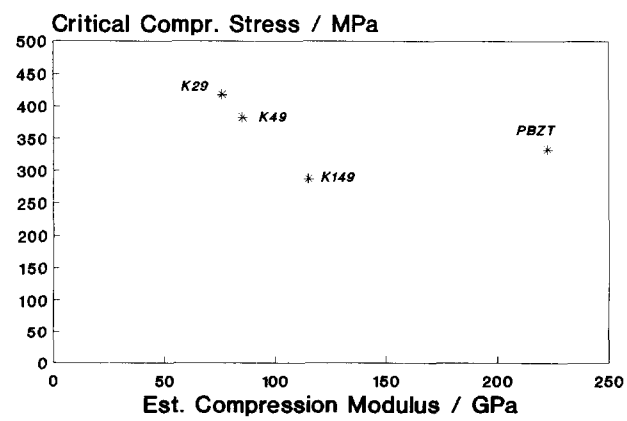

Figure 14 Critical compressive stress as a function of estimated compressive Young's modulus for Kevlar 49, Kevlar 29, Kevlar 149 and PBZT fibres

CONCLUSIONS

The bending beam technique combined with LRS can be used to follow the molecular deformation of fibres in both tension and compression. Important parameters such as the critical compressive strain to failure, the deformation at the post-failure region and the amount of modulus softening in compression can be determined. In addition, estimates of the compression modulus and the critical compressive stress to failure can be derived assuming a linear stress–strain relationship in the elastic region.

The results presented confirmed that LCP fibres 'yield' in compression by microbuckling. The compressive strength of aramid fibres decreases as the modulus increases, whereas new LCP fibres of high moduli still suffer from an inherent low compressive strength. The compression modulus appears to be lower than the tensile modulus and this effect is more pronounced for fibres exhibiting relatively high axial stiffness in tension.

ACKNOWLEDGEMENTS

We would like to thank E. I. du Pont de Nemours Co. (Wilmington) for supplying the Kevlar fibres and for financial support, and the Royal Aerospace Establishment (UK) for supplying the PBZT fibres. One of us (CV) would like to thank the Pateras Foundation for a scholarship. Nick Melanitis is also thanked for assistance with the experiment.

REFERENCES

1 Kumar, S. and Helminiak, T. E. *MRS Symp.* 1988, **134**, 363
2 DeTeresa, S. J., Porter, R. S. and Farris, R. J. *J. Mater. Sci.* 1985, **20**, 1645
3 DeTeresa, S. J., Porter, R. S. and Farris, R. J. *J. Mater. Sci.* 1988, **23**, 1886
4 Sinclair, D. *J. Appl. Phys.* 1950, **21**, 380
5 Jones, W. R. and Johnson, J. W. *Carbon* 1971, **9**, 645
6 Greenwood, J. M. and Rose, P. G. *J. Mater. Sci.* 1974, **9**, 1809
7 Hawthorne, H. M. and Teghtsoonian, E. *J. Mater. Sci.* 1975, **10**, 41
8 Allen, S. R. *J. Mater. Sci.* 1987, **22**, 853
9 DeTeresa, S. J., Porter, R. S. and Farris, R. J. *J. Mater. Sci.* 1988, **23**, 1886
10 Jahankhani, H. and Galiotis, C. in 'Interfaces in Polymer, Ceramic and Metal Matrix Composites' (Ed. H. Ishida), Elsevier, New York, 1988, p. 107
11 Van der Zwaag, S. and Kampschoer, G. 'Integration of Fundamental Polymer Sci. & Technology', 2nd Edn (Eds P. J. Lemstra and L. Kleintjens), Elsevier Applied Science, Oxford, 1988, p. 545
12 Dobb, M. G., Johnson, D. J. and Park, C. R. *J. Mater. Sci.* 1990, **25**, 829
13 Timoshenko, S. P. and Gere, J. M. 'Theory of Elastic Stability', McGraw-Hill, New York, 1961
14 Melanitis, N. and Galiotis, C. *J. Mater. Sci.* 1990, **25**, 5081
15 Galiotis, C. *PhD Thesis* University of London, 1982
16 Galiotis, C., Young, R. J., Yeung, P. H. J. and Batchelder, D. N. *J. Mater. Sci.* 1984, **19**, 3640
17 Galiotis, C., Robinson, I. M., Young, R. J., Smith, B. J. E. and Batchelder, D. N. *Polym. Commun.* 1985, **26**, 354
18 Galiotis, C. and Batchelder, D. N. *J. Mater. Sci. Lett.* 1988, **7**, 545
19 Day, R. J., Robinson, I. M., Zakikhani, M. and Young, R. J. *Polymer* 1987, **28**, 1833
20 Kim, P. K., Chang, C. and Hsu, S. L. *Polymer* 1986, **27**, 34
21 Shen, D. Y., Venkatesh, G. M., Burchell, D. J., Shu, P. H. C. and Hsu, S. L. *J. Polym. Sci., Polym. Phys. Edn* 1982, **20**, 509
22 Vlattas, C. and Galiotis, C. to be published
23 Van der Zwaag, S., Northolt, M. G., Young, R. J., Robinson, I. M., Galiotis, C. and Batchelder, D. N. *Polym. Commun.* 1987, **28**, 276